SCATTERING FROM A THIN MAGNETIC LAYER WITH A PERIODIC LATERAL MAGNETIZATION: APPLICATION TO ELECTROMAGNETIC ABSORBERS

J. Ramprecht and M. Norgren

Division of Electromagnetic Engineering
School of Electrical Engineering
Royal Institute of Technology
Teknikringen 33, SE-100 44 Stockholm, Sweden

D. Sjöberg

Department of Electrical and Information Technology
Electromagnetic Theory
Lund University
Box 118, SE-221 00 Lund, Sweden

Abstract—A magnetized thin layer mounted on a PEC surface is considered as an alternative for an absorbing layer. The magnetic material is modeled with the Landau-Lifshitz-Gilbert equation, with a lateral static magnetization having a periodic variation along one lateral direction. The scattering problem is solved by means of an expansion into Floquet-modes, a propagator formalism and wave-splitting. Numerical results are presented, and for parameter values close to the typical values for ferro- or ferrimagnetic media, reflection coefficients below $-20\,\text{dB}$ can be achieved for the fundamental mode over the frequency range 1–4 GHz, for both polarizations. It is found that the periodicity of the medium makes the reflection properties for the fundamental mode almost independent of the azimuthal direction of incidence, for both normally and obliquely incident waves.

1. INTRODUCTION

For absorption of electromagnetic waves, magnetic media have some features making them more appropriate than their electric counterparts. For example, when reducing the reflection from a PEC surface, a thin magnetically lossy sheet can be placed directly onto

the surface whereas the corresponding electrically lossy sheet must be suspended a quarter of a wavelength from the surface by using an additional dielectric layer. Hence, magnetic media has the possibility to offer designs with larger bandwidth and less space occupancy than electric media.

Using a medium with a scalar permeability, efficient absorption can be obtained if the permeability is large and its imaginary (lossy) part dominates over its real part [1]. The larger the lossy permeability is the thinner one can make the absorbing layer. For that purpose, composite media realized as laminated structures of ferromagnetic thin films is a very promising alternative, since such media have among the highest possible permeabilities in the microwave region reported up to date. Quite recent experimental investigations [2, 3] report loss parts of the permeability in the order 200 or more in the lower microwave band, for frequencies ranging approximately from 1 to 10 GHz.

A suitable phenomenological model for ferromagnetic media is the Landau-Lifshitz-Gilbert (LLG) equation [4], which for small-signal analysis of microwave fields is linearized around a static equilibrium solution for the magnetization. Due to surface effects the static magnetization in ferromagnetic thin films is predominantly oriented in the lateral directions. By spontaneous arrangements, subject to geometrical constraints, or by externally enforced magnetic fields [5, 6] the magnetization assumes certain patterns, varying in both the lateral and normal directions [7–9]. Such magnetizations result in a small-signal permeability that is both anisotropic and heterogeneous.

Engineered thin film magnetic layers with the magnetization vector organized in certain patterns is a way to utilize the ubiquitous anisotropy in order to obtain desired reflection properties, when the layer is exposed to fields of different polarizations. From the point of view of radar cross section reduction (RCSR) it is usually desired to reduce the reflection for both polarizations of the incident wave, but in other applications it may be desired that the layer absorbs efficiently for only one polarization, like e.g., the suppression of surface waves in array antennas and other periodic structures [10].

In this paper we investigate theoretically the possibility of achieving efficient RCSR using a magnetized layer (presumably realized as a laminate of ferromagnetic thin films) having a lateral magnetization that varies periodically along one of the lateral directions. First the conditions on a magnetic Salisbury screen, the LLG-equation and the small-signal model for the gyrotropic permeability are reviewed. Then, the absorption efficiencies, under illumination in the normal direction, using two special directions of magnetization are discussed, *viz.* a normally directed magnetization

and a laterally directed homogeneous magnetization, and conclude that the laterally magnetized layer is potentially more advantageous. From that, we turn to a periodically varying lateral magnetization and derive the resulting heterogeneous permeability tensor, with parameter values mimicking a magnetic conductivity model. Next, the method for solving the scattering problem is presented: a spectral representation in terms of Floquet-modes for the lateral dependencies, a propagator method for mapping the fields in the normal direction and a wave-splitting technique for extracting the reflection coefficients for the Floquet-modes. Numerical results are presented, for the dependencies of the reflection coefficients on the polar and azimuthal angles of incidence, the saturation magnetization and the loss parameter. The sensitivity of an RCSR design for deviations from the magnetic conductivity model is also investigated.

2. THE MAGNETIC SALISBURY SCREEN

We define an absorbing layer to be thin if $d \ll \lambda$, where d is the thickness of the layer and λ is the wavelength in the exterior region. The backscattered field from normally impinging waves on an isotropic thin lossy sheet above a PEC surface can be completely extinct provided [1, p. 337]

$$\sigma_{\mathrm{m}} d = \eta_0 \tag{1}$$

$$\mu'' \gg \mu' \tag{2}$$

where $\sigma_{\mathrm{m}} \equiv \omega\mu_0\mu''$, η_0 is the vacuum wave impedance, ω the angular frequency and μ'' the imaginary part of the relative permeability.

The operation of this design is based on interaction inside the layer rather than matching of the impedance at the front surface. Thus, the layer must be penetrable, $i.e.$, $d \ll \delta$, where δ is the penetration depth of the layer. Therefore, the conditions above must be supplemented with another condition. Assume that the relative permittivity, ε, is real valued and that the conditions above are fulfilled, whereby the wave number becomes

$$k = k_0\sqrt{\varepsilon\mu} \approx k_0\sqrt{\frac{\varepsilon\mu''}{2}}(1+\mathrm{i}) \Rightarrow \delta = k_0^{-1}\sqrt{\frac{2}{\varepsilon\mu''}},$$

where $k_0 = \omega\sqrt{\varepsilon_0\mu_0}$ is the free space wave number.

Using (1) and $d \ll \delta$ finally gives us a third condition

$$\sqrt{\frac{\varepsilon}{2\mu''}} \ll 1 \quad \Rightarrow \quad \mu'' \gg \varepsilon \tag{3}$$

In order to obtain extinction over a broad frequency range, we see from condition (1) that a frequency dependent permeability with $\mu'' \propto 1/\omega$ is desirable. This means, analogous to the electric conductivity model, that the material exhibits a magnetic conductivity σ_{m}. A material with the above characteristics can provide efficient absorption of electromagnetic energy over a very wide frequency range. Such a design is sometimes referred to as a magnetic Salisbury screen.

However, magnetic media are often anisotropic, and the magnetization depends on the magnetic field in a complicated way. This anisotropy may be an undesired effect since good absorption for both polarization of the wave is often wanted. Hence, accurate modeling of magnetic media requires methods that handles anisotropy.

3. EQUATION OF MOTION

In ferromagnetic media, the magnetic moments of the atoms tend to be aligned with each other in certain directions. This alignment is due to a strong coupling between the magnetic moments in neighboring atoms. The precise mechanism of this coupling is not easy to understand, but may be modeled in a phenomenological way. The dynamics of the magnetic moment per unit volume, $i.e.$, the magnetization $\boldsymbol{M}$, is described by the Landau-Lifshitz-Gilbert (LLG) equation [4, 11, 12]

$$\frac{\partial \boldsymbol{M}}{\partial t} = -\gamma\mu_0 \boldsymbol{M} \times \boldsymbol{H}_{\mathrm{eff}} + \alpha\frac{\boldsymbol{M}}{M_{\mathrm{S}}} \times \frac{\partial \boldsymbol{M}}{\partial t} \tag{4}$$

where $\gamma = 1.759 \cdot 10^{11}$ C/kg is the gyromagnetic ratio and μ_0 is the permeability of vacuum. The dimensionless factor α is related to the losses and is typically of the order of $\alpha \approx 0.1$. The right hand side is orthogonal to $\boldsymbol{M}$, which results in that the magnitude of the magnetization is preserved, $|\boldsymbol{M}| = M_{\mathrm{S}}$, where M_{S} is the saturation magnetization. The magnitude of M_{S} is typically in the interval $10^5 - 2 \cdot 10^6$ A/m [13].

The effective field $\boldsymbol{H}_{\mathrm{eff}}$ has several contributions, of which some are of quite different origin than that of the classical magnetic field described by the Maxwell equations [4, 6]. Besides from the classical magnetic field, the effective field takes effects like exchange interactions and magnetocrystalline anisotropy into account. Since we in this paper mainly investigate the effect of the large scale periodicity of the medium, the equation of motion is kept simple by only taking into account the classical magnetic field.

4. THE SMALL-SIGNAL PERMEABILITY DYADIC

When the magnetic specimen is subjected to a weak time-varying magnetic field, Equation (4) may be linearized around the static solution $\boldsymbol{M}_0$. For this purpose we assume that the classical magnetic field has one static bias part and one signal part (time convention $\mathrm{e}^{-\mathrm{i}\omega t}$), with the resulting splitting of the magnetization

$$\boldsymbol{H} = \boldsymbol{H}_0 + \boldsymbol{H}_1\mathrm{e}^{-\mathrm{i}\omega t}, \quad \boldsymbol{M} = \boldsymbol{M}_0 + \boldsymbol{M}_1\mathrm{e}^{-\mathrm{i}\omega t} \tag{5}$$

where index 0 corresponds to fields constant in time, and time harmonic fields are indexed by 1. The magnetization $\boldsymbol{M}_0$ is the static solution of (4) to an applied static magnetic field $\boldsymbol{H}_0$. The small-signal magnetic field $\boldsymbol{M}_1$ then represents small deviations from the static magnetization due to the small-signal field $\boldsymbol{H}_1$. The static magnetic field also consists of two part: $\boldsymbol{H}_0 = \boldsymbol{H}_0^{\mathrm{e}} + \boldsymbol{H}_{\boldsymbol{M}_0}$, where $\boldsymbol{H}_0^{\mathrm{e}}$ is an external applied static magnetic field and $\boldsymbol{H}_{\boldsymbol{M}_0}$ is the magnetic field due to the static magnetization $\boldsymbol{M}_0$. For the special case of a spheroidal particle immersed in a static homogeneous external field $\boldsymbol{H}_0^{\mathrm{e}}$, the particle is uniformly magnetized, and the total static field within the particle can be shown to be

$$\boldsymbol{H}_0 = \boldsymbol{H}_0^{\mathrm{e}} + \boldsymbol{H}_{\boldsymbol{M}_0} = \boldsymbol{H}_0^{\mathrm{e}} - \mathbf{N}_{\mathrm{d}}\boldsymbol{M}_0 \tag{6}$$

where $\mathbf{N}_{\mathrm{d}}$ is the demagnetization tensor for the particle. Letting $\boldsymbol{M}_0 = M_{\mathrm{S}}\boldsymbol{m}_0$, where the unit vector $\boldsymbol{m}_0$ is the direction of the static magnetization, and following the procedure in [6] we obtain a small signal permeability

$$\boldsymbol{\mu} = \mu_{\mathrm{m}}\boldsymbol{m}_0\boldsymbol{m}_0 + \mu_{\mathrm{t}}(\mathbf{I} - \boldsymbol{m}_0\boldsymbol{m}_0) + \mathrm{i}\mu_{\mathrm{g}}\boldsymbol{m}_0 \times \mathbf{I} \tag{7}$$

where $\mathbf{I}$ is the identity dyadic and the coefficients are

$$\mu_{\mathrm{m}}(\omega) = 1 \tag{8}$$

$$\mu_{\mathrm{t}}(\omega) = 1 + \frac{\beta - \mathrm{i}\alpha\omega/\omega_{\mathrm{S}}}{(\beta - \mathrm{i}\alpha\omega/\omega_{\mathrm{S}})^2 - (\omega/\omega_{\mathrm{S}})^2} \tag{9}$$

$$\mu_{\mathrm{g}}(\omega) = \frac{\omega/\omega_{\mathrm{S}}}{(\beta - \mathrm{i}\alpha\omega/\omega_{\mathrm{S}})^2 - (\omega/\omega_{\mathrm{S}})^2} \tag{10}$$

with

$$\omega_{\mathrm{S}} = \gamma\mu_0 M_{\mathrm{S}} \tag{11}$$

The constant β depends on the shape of the specimen and on the external bias field $\boldsymbol{H}_0^{\mathrm{e}}$. For a thin layer biased in the normal direction

$\beta = |\boldsymbol{H}_0^{\mathrm{e}}|/M_{\mathrm{S}} - 1$ and when biased in the plane $\beta = |\boldsymbol{H}_0^{\mathrm{e}}|/M_{\mathrm{S}}$. Furthermore, from the typical range of values for M_{S}, we see that the intrinsic precession frequency, $f_{\mathrm{S}} = \omega_{\mathrm{S}}/2\pi$, typically is in the range from 3 to 70 GHz.

5. SPECIAL CASES OF MAGNETIZATION

The approach for achieving a broadband absorber will be to investigate whether the anisotropic media described by (7) can approximately mimic the magnetic Salisbury screen. We will review the two special cases when the static magnetization $\boldsymbol{M}_0$ is either in the normal direction of the layer surface or in the lateral direction; see Figure 1. We choose z as the normal direction and (x, y) as lateral directions. It is also assumed that layer thickness d is much smaller than the lateral dimensions of the layer.
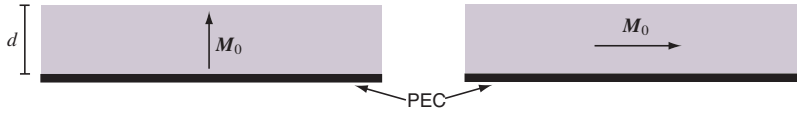

Figure 1. Two special cases of the static magnetization direction inside a layer of thickness d. The left figure illustrates the case when the magnetization is in the normal direction and the right corresponds to the case of lateral magnetization.

5.1. Normal Magnetization

The reflection properties for this case has been studied in [6] and the results obtained are briefly summarized here. With a strong enough bias field $\boldsymbol{H}_0^{\mathrm{e}}$ in the normal direction, a static solution $\boldsymbol{M}_0 = M_{\mathrm{S}}\hat{\boldsymbol{z}}$ of (4) is obtained. The permeability dyadic (7) then has the following matrix representation

$$\boldsymbol{\mu} = \begin{pmatrix} \mu_{\mathrm{t}} & -\mathrm{i}\mu_{\mathrm{g}} & 0 \\ \mathrm{i}\mu_{\mathrm{g}} & \mu_{\mathrm{t}} & 0 \\ 0 & 0 & \mu_{\mathrm{m}} \end{pmatrix} \tag{12}$$

This small-signal permeability represents a gyrotropic medium and its invariance under rotations around the z-axis yields the attractive property that reflection of normally incident plane waves are unchanged if the layer is rotated around the z-axis. It is well known that the eigenmodes for propagation along the magnetization direction

(z-axis) in such a medium correspond to circularly polarized waves. The eigenvalues of the permeability dyadic corresponding to these circularly polarized eigenmodes are given by

$$\mu_\pm = \mu_\mathrm{t} \pm \mu_g \tag{13}$$

where the different signs correspond to the mode being either right or left hand circularly polarized. In terms of wave-number and wave-impedance, each mode experiences an effective permeability given by its associated eigenvalue. This means, for instance, that left and right hand circularly polarized waves have different phase velocities.

With the aid of the external bias field $\boldsymbol{H}_0^\mathrm{e}$, via the parameter β, the behavior of the material can be altered and it is shown in [6] that the largest bandwidth is obtained when $\beta \to 0$, $i.e.$, $|\boldsymbol{H}_0^\mathrm{e}| = M_\mathrm{S}$, whereby the effective permeabilities become

$$\mu_\pm = 1 \pm \frac{\omega_\mathrm{S}}{\omega\left(1+\alpha^2\right)} + \mathrm{i}\frac{\alpha\omega_\mathrm{S}}{\omega\left(1+\alpha^2\right)} \tag{14}$$

From this we see that the imaginary part of the effective permeabilities have exactly the frequency dependence required for a broadband matching using condition (1) and that the losses can be described by a magnetic conductivity

$$\sigma_\mathrm{m} = \mu_0\frac{\alpha}{1+\alpha^2}\omega_\mathrm{S} \tag{15}$$

Using this expression in (1), we see that in order to obtain a thin absorber, a large σ_m is needed. Therefore, large values for the loss parameter α and the saturation magnetization M_S is desirable. However, for condition (2) to be fulfilled, one can show that the loss parameter must fulfill

$$1 \ll \alpha \ll \frac{\omega_\mathrm{S}}{\omega} \tag{16}$$

Hence, for this material to behave approximately as an isotropic material in a Salisbury screen, unrealistically high values of α are required and even though they could be realized ω must be exceedingly smaller than ω_S, $i.e.$, well below the microwave region.

Additional disadvantages with this design is that a very strong external bias field $\boldsymbol{H}_0^\mathrm{e}$ is needed in order to magnetize the layer in the normal direction [14, 15]. To obtain a stable static magnetization in the normal direction a positive β is required, $i.e.$, $|\boldsymbol{H}_0^\mathrm{e}| > M_\mathrm{S}$, which can be difficult to achieve practically. In [6], it is also found that the reflection properties when $\beta \approx 0$ are very sensitive to changes in β,

making it difficult to control the material with an external bias field. Furthermore, only one of the circularly polarized modes will experience substantial absorption in the material. This is due to the fact that the LLG equation describes a precessive behavior of the magnetization and only the mode that works with this precession will be damped in an efficient way. Hence, when combined into linearly polarized modes, the co-polarized reflection can be reduced efficiently only by allowing the cross-polarized reflection to become substantial [6].

5.2. Lateral Magnetization

In the absence of an external bias field it will be energetically favorable for the magnetization to assume a lateral direction in the layer. The exact direction of the magnetization can be controlled by a bias field in the (x, y) plane, forcing the magnetization to align with the bias field. With a lateral bias field such that $\boldsymbol{M}_0 = M_S \hat{\boldsymbol{x}}$ the permeability dyadic (7) now has the following matrix representation

$$\boldsymbol{\mu} = \begin{pmatrix} \mu_\mathrm{m} & 0 & 0 \\ 0 & \mu_\mathrm{t} & -\mathrm{i}\mu_\mathrm{g} \\ 0 & \mathrm{i}\mu_\mathrm{g} & \mu_\mathrm{t} \end{pmatrix} \tag{17}$$

with $\beta = |\boldsymbol{H}_0^\mathrm{e}|/M_S$. In this case, the eigenmodes associated with a normally incident plane wave are linearly polarized. The mode with the magnetic field in the x-direction is not affected by the parameters in the LLG-equation, and thus can not be treated for absorption as described in this paper. The other mode experiences the effective permeability [16, p. 459]

$$\mu_\mathrm{eff} = \mu_\mathrm{t} - \mu_\mathrm{g}^2/\mu_\mathrm{t} \tag{18}$$

We once again examine the case when $\beta \to 0$, $i.e.$, $|\boldsymbol{H}_0^\mathrm{e}| \to 0$, whereby

$$\mu_\mathrm{g}(\omega) = -\frac{\omega_\mathrm{S}}{(1+\alpha^2)\omega}, \quad \mu_\mathrm{t}(\omega) = 1 + \frac{\mathrm{i}\alpha\omega_\mathrm{S}}{(1+\alpha^2)\omega} = 1 - \mathrm{i}\alpha\mu_\mathrm{g} \tag{19}$$

Introducing $t = -\dfrac{1}{\alpha\mu_\mathrm{g}}$ and assuming $t \ll 1$ we obtain

$$\mu'_\mathrm{eff} \approx 1 - \frac{1}{\alpha^2}, \quad \mu''_\mathrm{eff} \approx \frac{1}{t}\left(1 + \frac{1}{\alpha^2}\right) = \frac{\omega_\mathrm{S}}{\alpha\omega} \gg 1 \tag{20}$$

where $\mu_\mathrm{eff} = \mu'_\mathrm{eff} + \mathrm{i}\mu''_\mathrm{eff}$. From this it is seen that if $t \ll 1$, then condition (1), (2) and, quite likely, also condition (3) approximately

hold, regardless of the value of α. The condition $t \ll 1$ is equivalent with

$$\omega \ll \frac{\alpha}{1 + \alpha^2} \omega_{\mathrm{S}} \tag{21}$$

Thus, for small enough frequencies this material behaves approximately as the desired material in a Salisbury screen, no matter what value α assumes. Unfortunately, this only applies for one of the polarizations. However, unlike the previous case of magnetization in the normal direction, no bias field is required in order to obtain $\beta = 0$ and thus fulfilling the Salisbury conditions.

We also note from (20) that for $t \ll 1$, the magnetic conductivity becomes

$$\sigma_{\mathrm{m}} = \mu_0 \frac{\omega_{\mathrm{S}}}{\alpha} \tag{22}$$

Once again returning to (1), we find that for this case a large saturation magnetization M_{S} but a *small* loss parameter α is needed in order to obtain a thin absorber. However, to obtain good absorption in the high frequency range a large α is desirable, as seen from (21). Hence, thin absorbers may have difficulties in performing well in the high frequency range.

6. PERIODICALLY ROTATING LATERAL MAGNETIZATION

The results in the previous section implies that for realistic values on the loss parameter α and the external bias field $\boldsymbol{H}_0^{\mathrm{e}}$, an approximation to the magnetic Salisbury screen that provides good absorption over a wide frequency range can be obtained only for the laterally magnetized medium and then only for one of the linearly polarized eigenmodes. Inspired by that case, we consider using a lateral magnetization that varies periodically. The hypothesis is to cancel out the anisotropy associated with the magnetization direction and thus achieving decent absorption for both polarizations.

We assume that $\boldsymbol{M}_0$ is periodic in the x-direction, with the following dependence

$$\boldsymbol{M}_0 = M_{\mathrm{S}} \left[\cos \left(\frac{2\pi x}{a} \right) \hat{\boldsymbol{x}} + \sin \left(\frac{2\pi x}{a} \right) \hat{\boldsymbol{y}} \right] \tag{23}$$

where a is the periodicity, the width of the unit cell. As before, $|\boldsymbol{M}_0| = M_{\mathrm{S}}$, but the direction now changes along the x-direction; see Figure 2.
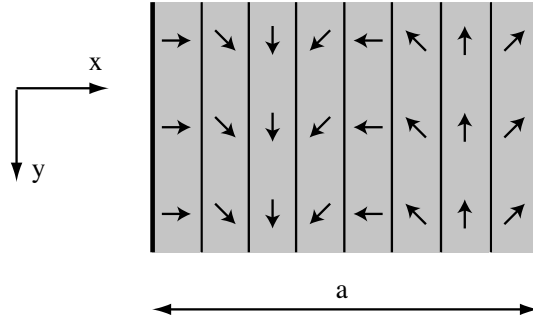
Figure 2. One period in an approximation to a layer with the magnetization (23). Thin homogeneously magnetized stripes with progressively changing magnetization.

The static fields $\boldsymbol{H}_0$ and $\boldsymbol{M}_0$ must simultaneously satisfy the LLG-equation and the static Maxwell equations with the appropriate boundary conditions [15, p. 27]. These combined equations are typically nonlinear and difficult to solve even numerically. Thus in general one cannot specify $\boldsymbol{M}_0$, but instead has to solve a non-linear boundary value problem to find stable periodic solutions. To avoid this, (23) is tacitly considered as a qualified guess, and the resulting fields will be determined in order to see the deviation from the ideal case.

Assume that the layer is between $0 < z < d$, with a PEC surface at $z = d$ and air in the region $z < 0$. With $\pi d/a \ll 1$, *i.e.*, a very thin layer compared with its periodicity, one can show that to first order in $\pi d/a$ the magnetic field inside a layer is given by (see Appendix A)

$$\boldsymbol{H}_0 = M_{\mathrm{S}} \left[-\frac{\pi d}{a} \cos\left(\frac{2\pi x}{a}\right) \hat{\boldsymbol{x}} + \frac{2\pi}{a} \left(z - \frac{d}{2}\right) \sin\left(\frac{2\pi x}{a}\right) \hat{\boldsymbol{z}} \right], \ \ 0 < z < d \ (24)$$

In the limit $d \to 0$ we obtain $\boldsymbol{H}_0 = 0$ (assuming $\boldsymbol{H}_0^{\mathrm{e}} = 0$). Thus, in this limit (23) and (24) satisfy both the LLG-equation and the static Maxwell equations, and for $\pi d/a \ll 1$ this solution will be assumed to hold approximately. Also, again we obtain the case $\beta = 0$ and the simplified expressions (19) for μ_{g} and μ_{t}.

Introduce $\phi = 2\pi x/a$, the direction-angle of $\boldsymbol{M}_0$ measured from the $+x$-axis, and a local coordinate system rotated around the z-axis so that the local x-direction is along $\boldsymbol{M}_0$. In this local system the

permeability tensor is given by

$$\boldsymbol{\mu}' = \begin{pmatrix} \mu_\mathrm{m} & 0 & 0 \\ 0 & \mu_\mathrm{t} & -\mathrm{i}\mu_\mathrm{g} \\ 0 & \mathrm{i}\mu_\mathrm{g} & \mu_\mathrm{t} \end{pmatrix} \tag{25}$$

Using a similarity transformation we obtain the following heterogeneous permeability tensor in the main coordinate system

$$\boldsymbol{\mu}(\phi(x)) = \mathbf{R}^{-1}\boldsymbol{\mu}'\mathbf{R} =$$
$$\begin{pmatrix} \mu_\mathrm{m}\cos^2\phi + \mu_\mathrm{t}\sin^2\phi & (\mu_\mathrm{m} - \mu_\mathrm{t})\sin\phi\cos\phi & \mathrm{i}\mu_\mathrm{g}\sin\phi \\ (\mu_\mathrm{m} - \mu_\mathrm{t})\sin\phi\cos\phi & \mu_\mathrm{m}\sin^2\phi + \mu_\mathrm{t}\cos^2\phi & -\mathrm{i}\mu_\mathrm{g}\cos\phi \\ -\mathrm{i}\mu_\mathrm{g}\sin\phi & \mathrm{i}\mu_\mathrm{g}\cos\phi & \mu_\mathrm{t} \end{pmatrix} \tag{26}$$

where

$$\mathbf{R} = \begin{pmatrix} \cos\phi & \sin\phi & 0 \\ -\sin\phi & \cos\phi & 0 \\ 0 & 0 & 1 \end{pmatrix} \tag{27}$$

7. PROPAGATION IN A LATERALLY PERIODIC ANISOTROPIC LAYER

In [17], this problem is solved in detail for isotropic media, whereas the case of bianisotropic media is merely outlined. Here we fill in some details for the magnetically anisotropic case where the relative permeability $\boldsymbol{\mu}(x)$ is periodic in the x-direction. Although it is reasonable to assume that also the permittivity dyadic is in general periodic, we restrict this study to magnetic parameters only, wherefore the relative permittivity is assumed to be isotropic and homogeneous i.e., $\boldsymbol{\varepsilon} = \varepsilon\mathbf{I}$.

7.1. Fundamental Equation

In cartesian components, the time-harmonic Maxwell's equations $\nabla \times \boldsymbol{E} = \mathrm{i}\omega\mu_0\boldsymbol{\mu}\boldsymbol{H}$ and $\nabla \times \boldsymbol{H} = -\mathrm{i}\omega\varepsilon_0\boldsymbol{\varepsilon}\boldsymbol{E}$, become

$$\frac{\partial E_z}{\partial y} - \frac{\partial E_y}{\partial z} = \mathrm{i}\omega\mu_0(\mu_{11}H_x + \mu_{12}H_y + \mu_{13}H_z) \tag{28}$$

$$\frac{\partial E_x}{\partial z} - \frac{\partial E_z}{\partial x} = \mathrm{i}\omega\mu_0(\mu_{21}H_x + \mu_{22}H_y + \mu_{23}H_z) \tag{29}$$

$$\frac{\partial E_y}{\partial x} - \frac{\partial E_x}{\partial y} = \mathrm{i}\omega\mu_0(\mu_{31}H_x + \mu_{32}H_y + \mu_{33}H_z) \tag{30}$$

and

$$\frac{\partial H_z}{\partial y} - \frac{\partial H_y}{\partial z} = -\mathrm{i}\omega\varepsilon_0\varepsilon E_x \tag{31}$$

$$\frac{\partial H_x}{\partial z} - \frac{\partial H_z}{\partial x} = -\mathrm{i}\omega\varepsilon_0\varepsilon E_y \tag{32}$$

$$\frac{\partial H_y}{\partial x} - \frac{\partial H_x}{\partial y} = -\mathrm{i}\omega\varepsilon_0\varepsilon E_z \tag{33}$$

respectively. Using (30) and (33), the z-components of the fields become

$$E_z = \frac{\mathrm{i}}{\omega\varepsilon_0\varepsilon}\left(\frac{\partial H_y}{\partial x} - \frac{\partial H_x}{\partial y}\right) \tag{34}$$

$$H_z = \mu_{33}^{-1}\left[\frac{-\mathrm{i}}{\omega\mu_0}\left(\frac{\partial E_y}{\partial x} - \frac{\partial E_x}{\partial y}\right) - \mu_{31}H_x - \mu_{32}H_y\right] \tag{35}$$

Inserting this into (28), (29), (31) and (32), we obtain

$$\frac{\partial E_x}{\partial z} = \mathrm{i}\omega\mu_0[(\mu_{21} - \mu_{23}\mu_{33}^{-1}\mu_{31})H_x + (\mu_{22} - \mu_{23}\mu_{33}^{-1}\mu_{32})H_y]$$
$$+ \mu_{23}\mu_{33}^{-1}\left(\frac{\partial E_y}{\partial x} - \frac{\partial E_x}{\partial y}\right) + \frac{\partial}{\partial x}\left\{\frac{\mathrm{i}}{\omega\varepsilon_0\varepsilon}\left(\frac{\partial H_y}{\partial x} - \frac{\partial H_x}{\partial y}\right)\right\} \tag{36}$$

$$\frac{\partial E_y}{\partial z} = -\mathrm{i}\omega\mu_0\left[(\mu_{11} - \mu_{13}\mu_{33}^{-1}\mu_{31})H_x + (\mu_{12} - \mu_{13}\mu_{33}^{-1}\mu_{32})H_y\right]$$
$$- \mu_{13}\mu_{33}^{-1}\left(\frac{\partial E_y}{\partial x} - \frac{\partial E_x}{\partial y}\right) + \frac{\partial}{\partial y}\left\{\frac{\mathrm{i}}{\omega\varepsilon_0\varepsilon}\left(\frac{\partial H_y}{\partial x} - \frac{\partial H_x}{\partial y}\right)\right\} \tag{37}$$

$$\frac{\partial H_x}{\partial z} = -\mathrm{i}\omega\varepsilon_0\varepsilon E_y + \frac{\partial}{\partial x}\left\{\mu_{33}^{-1}\left[\frac{-\mathrm{i}}{\omega\mu_0}\left(\frac{\partial E_y}{\partial x} - \frac{\partial E_x}{\partial y}\right) - \mu_{31}H_x - \mu_{32}H_y\right]\right\} \tag{38}$$

$$\frac{\partial H_y}{\partial z} = \mathrm{i}\omega\varepsilon_0\varepsilon E_x + \frac{\partial}{\partial y}\left\{\mu_{33}^{-1}\left[\frac{-\mathrm{i}}{\omega\mu_0}\left(\frac{\partial E_y}{\partial x} - \frac{\partial E_x}{\partial y}\right) - \mu_{31}H_x - \mu_{32}H_y\right]\right\} \tag{39}$$

Assume an incident plane wave with the transversal wave-vector components

$$k_{0x} = k_0\sin\theta\cos\varphi, \quad k_{0y} = k_0\sin\theta\sin\varphi \tag{40}$$

where θ and φ are the polar and azimuthal angles of incidence. The tangential fields are expanded into the following Fourier-series (Floquet-modes)

$$E_i(x, y, z) = \mathrm{e}^{\mathrm{i}(k_{0x}x + k_{0y}y)}\sum_{n=-\infty}^{\infty} e_{i,n}(z)\mathrm{e}^{\mathrm{i}n\frac{2\pi}{a}x}, \quad i = x, y \tag{41}$$

$$H_i(x, y, z) = e^{i(k_{0x}x + k_{0y}y)} \sum_{n=-\infty}^{\infty} h_{i,n}(z) e^{in\frac{2\pi}{a}x}, \quad i = x, y \quad (42)$$

The expansions are truncated at $n = \pm N$ and the coefficients are collected into the vectors

$$\bar{e}_i(z) = \begin{pmatrix} e_{i,-N}(z) \\ \vdots \\ e_{i,N}(z) \end{pmatrix}, \quad \bar{h}_i(z) = \begin{pmatrix} h_{i,-N}(z) \\ \vdots \\ h_{i,N}(z) \end{pmatrix}, \quad i = x, y \quad (43)$$

From this we can rewrite (36)–(39) into a system of ordinary differential equations for the expansion coefficients (the fundamental equation)

$$\frac{d}{dz} \begin{pmatrix} \bar{e} \\ \bar{h} \end{pmatrix} = \begin{pmatrix} \mathbf{W}_{11} & \mathbf{W}_{12} \\ \mathbf{W}_{21} & \mathbf{W}_{21} \end{pmatrix} \begin{pmatrix} \bar{e} \\ \bar{h} \end{pmatrix}, \quad \bar{e} = \begin{pmatrix} \bar{e}_x \\ \bar{e}_y \end{pmatrix}, \bar{h} = \begin{pmatrix} \bar{h}_x \\ \bar{h}_y \end{pmatrix} \quad (44)$$

The matrices $\mathbf{W}_{ij}$ are determined by Fourier-expansions of the components of $\boldsymbol{\mu}$ as well as the tangential derivatives; detailed expressions are given in Appendix B.

7.2. Reflection

In this case, when the material is homogeneous in the z-direction, the propagator that maps the fields from the plane $z = z_1$ to the plane $z = z_2$ becomes [18]

$$\mathbf{P}(z_2, z_1) = e^{\mathbf{W}(z_2 - z_1)} \quad (45)$$

and the mapping from the rear surface to the front surface thus becomes

$$\begin{pmatrix} \bar{e}(0) \\ \bar{h}(0) \end{pmatrix} = \mathbf{P}(0, d) \begin{pmatrix} \bar{e}(d) \\ \bar{h}(d) \end{pmatrix} \equiv \begin{pmatrix} \mathbf{P}_{ee} & \mathbf{P}_{em} \\ \mathbf{P}_{me} & \mathbf{P}_{mm} \end{pmatrix} \begin{pmatrix} \bar{e}(d) \\ \bar{h}(d) \end{pmatrix} \quad (46)$$

With a PEC surface at $z = d$, we have $\bar{e}(d) = \mathbf{0}$ whereby (46) simplifies into

$$\bar{e}(0) = \mathbf{P}_{em}\bar{h}(d) \quad (47)$$
$$\bar{h}(0) = \mathbf{P}_{mm}\bar{h}(d) \quad (48)$$

In the region $z < 0$, a wave-splitting is applied whereby the fields are divided into $\pm z$-propagating TM- and TE-modes, with respect to the plane of incidence. Particularly, at the front surface we obtain

$$\begin{pmatrix} \bar{e}^+(0) \\ \bar{e}^-(0) \end{pmatrix} = \frac{1}{2} \begin{pmatrix} \boldsymbol{\Phi} & \mathbf{Z}\boldsymbol{\Phi} \\ \boldsymbol{\Phi} & -\mathbf{Z}\boldsymbol{\Phi} \end{pmatrix} \begin{pmatrix} \bar{e}(0) \\ \bar{h}(0) \end{pmatrix} \quad (49)$$

where

$$\bar{e}^+ = \begin{pmatrix} \bar{e}^+_{\mathrm{TM}} \\ \bar{e}^+_{\mathrm{TE}} \end{pmatrix}, \quad \bar{e}^- = \begin{pmatrix} \bar{e}^-_{\mathrm{TM}} \\ \bar{e}^-_{\mathrm{TE}} \end{pmatrix} \tag{50}$$

Here $\mathbf{\Phi}$ is a rotation matrix in the azimuthal direction and $\mathbf{Z}$ is an impedance matrix, containing the mode impedances for the Floquet-modes; see Appendix B.

The reflection coefficient matrix, $\mathbf{r}$, which relates the incident and reflected *tangential* electric fields, is defined from the relation

$$\bar{e}^- \equiv \mathbf{r}\bar{e}^+ \tag{51}$$

and since the tangential fields are continuous across the surface $z = 0$, insertion of (47) and (48) into (49) and the usage of (51) yield

$$\bar{e}^+ = \frac{1}{2}(\mathbf{\Phi P}_{\mathrm{em}} + \mathbf{Z\Phi P}_{\mathrm{mm}})\bar{h}(d) \tag{52}$$

$$\mathbf{r}\bar{e}^+ = \frac{1}{2}(\mathbf{\Phi P}_{\mathrm{em}} - \mathbf{Z\Phi P}_{\mathrm{mm}})\bar{h}(d) \tag{53}$$

wherefrom elimination of $\bar{h}(d)$ and the arbitrariness of $\bar{e}^+$ yield

$$\mathbf{r} = (\mathbf{\Phi P}_{\mathrm{em}} - \mathbf{Z\Phi P}_{\mathrm{mm}})(\mathbf{\Phi P}_{\mathrm{em}} + \mathbf{Z\Phi P}_{\mathrm{mm}})^{-1} \tag{54}$$

Since for the TM-modes, only the tangential projections of the electric field enters (51), the complete reflection coefficients are found by applying the corresponding back-projections on the components of $\mathbf{r}$ [17].

8. NUMERICAL REFLECTION RESULTS FOR A PERIODIC LAYER

The incoming plane wave that propagates in the $+z$-direction, with transversal wave-number given by (40), appears in the coefficients $e^+_{\mathrm{TM},0}$ and $e^+_{\mathrm{TE},0}$, for the fundamental mode (for $n \neq 0$ we have $e^+_{\mathrm{TM},n} = e^+_{\mathrm{TE},n} = 0$). The reflected fundamental modes appear in $e^-_{\mathrm{TM},0}$ and $e^-_{\mathrm{TE},0}$. Extracting the appropriate elements from the reflection matrix $\mathbf{r}$, we obtain the following 2×2 reflection coefficient matrix for the fundamental modes

$$\begin{pmatrix} \bar{e}^-_{\mathrm{TM},0} \\ \bar{e}^-_{\mathrm{TE},0} \end{pmatrix} = \begin{pmatrix} r_{\mathrm{TMTM},0} & r_{\mathrm{TMTE},0} \\ r_{\mathrm{TETM},0} & r_{\mathrm{TETE},0} \end{pmatrix} \begin{pmatrix} \bar{e}^+_{\mathrm{TM},0} \\ \bar{e}^+_{\mathrm{TE},0} \end{pmatrix} \tag{55}$$

For the special case of normal incidence ($\theta = 0$), the division into TM- and TE-modes is ambiguous since both modes become TEM. We then choose the polarizations of the modes such that their electric fields are in the x- and y-directions, respectively and denote TM(TE) by $X(Y)$.

In Figure 3 and Figure 4 we examine the reflection coefficients for different angles of incidence for a specific choice of material parameters. Besides from the desired case $\beta = 0$, we have in Figure 3 also included the influence of a small perturbation $\beta = 0.05$. For normal incidence we see from Figure 3(a) that r_{XX} and r_{YY} are quite equal in magnitude and between 0.8 and 4 GHz they are for $\beta = 0$ below -20 dB. The curves are not completely identical since the structure is periodic in the x-direction but constant in the y-direction. No cross-polarization was observed, within the numerical accuracy, i.e., $r_{XY} = r_{YX} = 0$.

For oblique incidence the reflection coefficients r_{TMTM} and r_{TETE} are no longer equal but still quite good broad band absorption is achieved and the cross polarization levels (not shown) remain below -20 dB for all frequencies. However, the results are very sensitive to disturbances in β for both angles of incidence, which means that such an absorber is unstable to small perturbing magnetic fields. Furthermore, from Figure 4 it is seen that the reflection coefficients are fairly independent of the azimuthal angle, i.e., the material behaves approximately as if isotropic. From the discussion following (22) we might expect that a decrease in the layer thickness d needs to be accompanied by an increase in the saturation magnetization M_S or
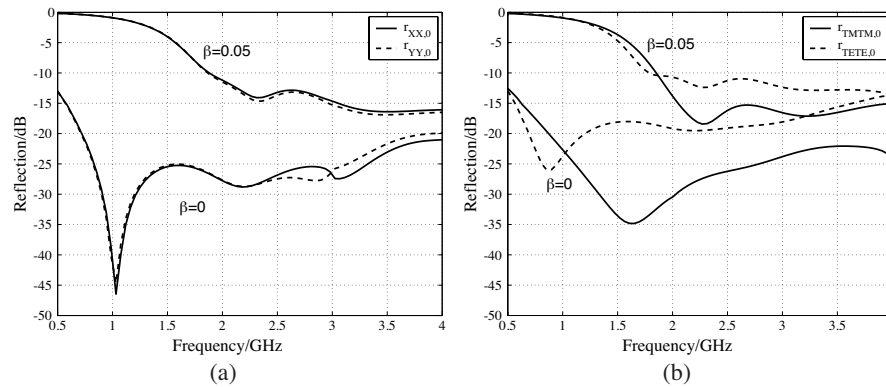

Figure 3. Reflection for different angles of incidence. The PEC-backed layer has a periodicity $a = 1 \cdot 10^{-1}$ m, thickness $d = 4.5 \cdot 10^{-3}$ m, $\alpha = 0.1$, $M_S = 5 \cdot 10^5$ A/m and an isotropic permittivity $\varepsilon = 5$. The maximum mode number $N = 26$. (a) $\theta = 0°$, $\varphi = 0°$. (b) $\theta = 30°$, $\varphi = 0°$.
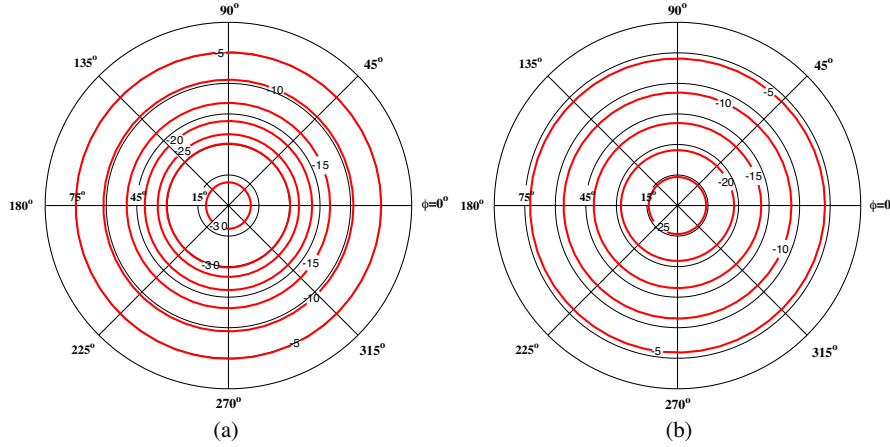
Figure 4. Curves of constant reflection (in dB) at $2\,\mathrm{GHz}$ with the polar coordinate in the radial direction. The PEC-backed layer has a periodicity $a = 1 \cdot 10^{-1}\,\mathrm{m}$, thickness $d = 4.5 \cdot 10^{-3}\,\mathrm{m}$, $\alpha = 0.1$, $M_\mathrm{S} = 5 \cdot 10^5\,\mathrm{A/m}$, $\beta = 0$ and an isotropic permittivity $\varepsilon = 5$. The maximum mode number $N = 26$. (a) r_{TMTM}, 0. (b) r_{TETE}, 0.
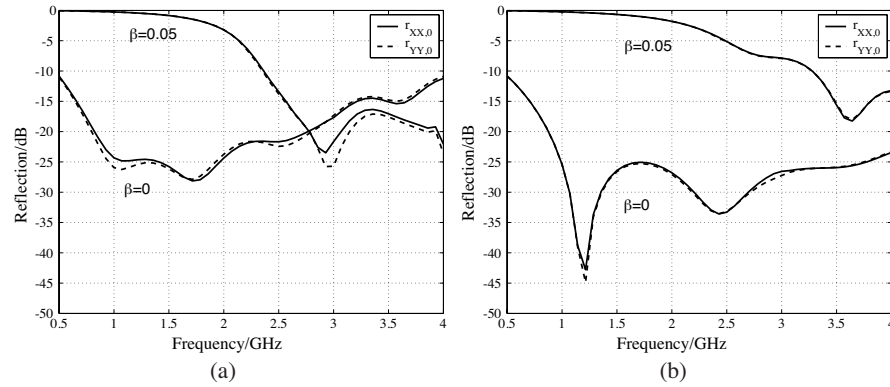

Figure 5. Reflection at normal incidence for different material parameters. The PEC-backed layer has a periodicity $a = 1 \cdot 10^{-1}\,\mathrm{m}$, thickness $d = 2.5 \cdot 10^{-3}\,\mathrm{m}$, and an isotropic permittivity $\varepsilon = 5$. The maximum mode number $N = 26$. (a) $\alpha = 0.05$, $M_S = 5 \cdot 10^5\,\mathrm{A/m}$. (b) $\alpha = 0.1$, $M_S = 1 \cdot 10^6\,\mathrm{A/m}$.

a decrease in the loss parameter α, in order to maintain low reflection for normal incidence. Indeed, this behavior is confirmed in Figure 5, which displays two variations of the design used in Figure 3(a) for

a reduced thickness: one changes only α, and one changes only M_S. Simultaneously increasing or decreasing α and M_S resulted in poorer results. However, in agreement with (21), when decreasing α we see from Figure 5(a) that the absorption at higher frequency is worse than in Figure 5(b) were α remains unchanged and M_S is increased. Thus, in terms of band width, it seems preferable to increase M_S rather than decreasing α when reducing the thickness of the absorber. Further, the results remain sensitive to small changes in β, and no cross polarization was observed. From Figure 6 we once again infer that the material is approximately isotropic. Also note that, for all cases of oblique incidence, the TM mode appears to have the best absorption.
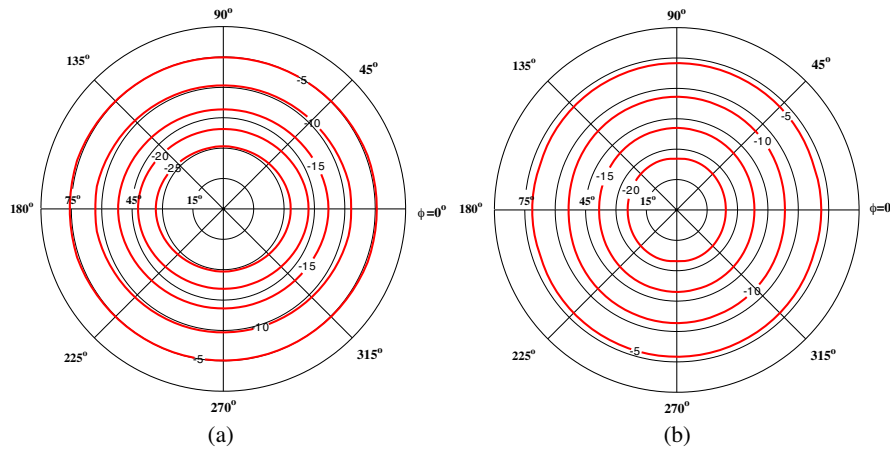

(a)

(b)

Figure 6. Curves of constant reflection (in dB) at $3.2\,\mathrm{GHz}$ with the polar coordinate in the radial direction. The PEC-backed layer has a periodicity $a = 1 \cdot 10^{-1}\,\mathrm{m}$, thickness $d = 2.5 \cdot 10^{-3}\,\mathrm{m}$, $\alpha = 0.1$, $M_S = 1 \cdot 10^{6}\,\mathrm{A/m}$, $\beta = 0$ and an isotropic permittivity $\varepsilon = 5$. The maximum mode number $N = 26$. (a) r_{TMTM}, 0. (b) r_{TETE}, 0.

Finally, here we have only considered the fundamental modes even though higher order modes start to propagate (in the $-z$-direction) within the frequency range investigated; in the numerical examples, at $3\,\mathrm{GHz}$ for normal incidence and below that for oblique incidence. For incidence in the xz-plane it may happen that a higher order mode is reflected in the opposite direction of the incoming wave. However, upon examination, the reflection coefficients for these higher order modes proved to remain below the $-20\,\mathrm{dB}$ level at all the frequencies presented here.

9. DISCUSSIONS AND CONCLUSIONS

The numerical examples indicate that composites and laminated films based on ferro- and ferrimagnetic media having a large saturation magnetization are possible candidates for thin absorbers operating in the lower microwave region. Unfortunately, they appear to be quite sensitive to perturbations in the parameter β, *i.e.*, to perturbing magnetic fields. To understand this consider moderate values of α. Then high losses in μ_t implies (cf. (19)) $\omega \ll \alpha\omega_\mathrm{S}$. In the general expressions (9), we see that β has minor influence if $\beta\omega_\mathrm{S} \ll \alpha\omega$, *i.e.*,

$$\beta \ll \alpha^2,$$

a condition that can be very difficult to reach uniformly within a layer.

Apart from being sensitive to deviations from $\beta = 0$, a periodically rotating lateral magnetization can "average out" the influence of anisotropy. Particularly, for normal incidence, with a layer of only a few millimeters in thickness, quite equal reflection coefficients for both polarizations with levels below $-20\,\mathrm{dB}$ are obtained for several octaves. For oblique incidence the reflection coefficients are different for the two polarizations, but almost independent of the azimuthal angle of incidence. Still, rather good absorption is achieved for several octaves up to $30°$ in the polar angle for both polarizations. However, when the wavelength of the incident wave is of the same order as the periodicity of the magnetization, *i.e.*, $\lambda \approx a$, we can no longer expect the material to behave as if isotropic, which is seen from Figure 6. Also, at these frequencies the higher order modes will most likely affect the isotropic behavior of the fundamental mode. Thus, in order to avoid these effects the absorber should be designed to operate for wavelengths $\lambda > a$.

A limitation of the numerical method is that for large n, the mode wave-numbers in the z-direction becomes $k_{z,n} \approx \mathrm{i}n2\pi/a$. Hence, the higher order evanescent modes will exhibit strong exponential growth/decay, resulting in ill-conditioned matrices. For thick layers, this may reduce the truncation number N considerably. However, in this paper where relatively thin layers are considered, the number of Floquet-modes used seems to be sufficient for the numerical results to converge before the matrices become ill-conditioned. As we have only considered a single-periodic layer, the trade-off between convergence and ill-conditionality must be re-examined in any extension of the present method to double-periodic layers. Securing the condition $\lambda > a$ by reducing the periodicity a the condition $\pi d/a \ll 1$ can be violated (even though the layer still is thin in terms of the wavelength, $d \ll \lambda$). In such a case, the numerical propagator method described becomes

inapplicable, and one must consider another method, like for example homogenizing the medium in the lateral directions [19].

In the present study we have overlooked the nonlinear magnetostatic problem that has to be solved in order to find the stable solutions of the static magnetization $\boldsymbol{M}_0$. In general, one then ends up with a static magnetization varying in the z-direction as well, and with all its cartesian components non-zero [7, 8]. The permeability tensor in (26) will then be stratified, *i.e.*, with an additional z-dependence. The stratified case can be solved by replacing the matrix exponential in (45) by numerical integration of Equation (44), which makes the method computationally slower, but the implementation is straight forward [16].

In summary, our results confirm that a periodical arrangement of the magnetization can lead to a desired property, in this case "isotropic" reflection of the fundamental mode. Hence, the concept of a periodically changing medium has potential usefulness when applied to other kinds of anisotropic, or even bianisotropic, media.

Furthermore, in this investigation we have only considered planar layers. It is also of interest to investigate weather the method of a lateral magnetization that varies periodically can be used to obtain an "isotropic" reflection from layers of more complex geometries designed as conformal to the surface. For example, the simplest non planar geometries are perhaps cylindrical structures. Applying a lateral periodically varying magnetization which is periodic along the cylinder will result in a RCS that is independent of the azimuthal angle. On the other hand applying a periodicity of the magnetization a long the azimuthal direction will result in a whole number of periods around the cylinder and an interaction with the cylindrical eigenmodes. The number of periods/turn will then most likely be crucial to the RCS dependence on the azimuthal angle. Typically a small period compared to the wavelength is required for the cylinder to behave approximately as isotropic.

APPENDIX A. THE MAGNETIC FIELD INSIDE A PERIODICALLY MAGNETIZED LAYER

Here, we present how the expression (24) for the field inside the layer is obtained from the expression (23) for the static magnetization. The method is general, and can thus be used for other forms of periodic static magnetizations.

The continuous variation in the static magnetization $\boldsymbol{M}_0$ gives rise to the magnetic volume charge density $\rho_{\mathrm{m}} = -\nabla \cdot \boldsymbol{M}_0$, and at surfaces where $\boldsymbol{M}_0$ varies discontinuously there will be a magnetic

surface charge density $\sigma_{\mathrm{m}} = \hat{\boldsymbol{n}}_{21} \cdot (\boldsymbol{M}_{0,1} - \boldsymbol{M}_{0,2})$.

Introducing a periodic Green's function $G(x, z; x', z')$ fulfilling

$$\left(\frac{\partial^2}{\partial x^2} + \frac{\partial^2}{\partial z^2} \right) G(x, z; x', z') = -\delta(x - x') \delta(z - z') \qquad \text{(A1)}$$

$$G(x + a, z; x', z') = G(x, z; x', z') \qquad \text{(A2)}$$

the periodic scalar magnetic potential is determined as

$$\Psi_0(x, z) = \int_0^a \mathrm{d}x' \int_{-\infty}^{\infty} \mathrm{d}z' G(x, z; x', z') \, \rho_{\mathrm{m}}(x', z')$$

$$+ \int_{\mathcal{C}} \mathrm{d}l' G(x, z; x', z') \, \sigma_{\mathrm{m}}(x', z') \qquad \text{(A3)}$$

where $\mathcal{C}$ denotes the set of surfaces (in one unit cell) where $\boldsymbol{M}_0$ is discontinuous.

Expanding $G(x, z; x', z')$ into the Fourier series

$$G(x, z; x', z') = \sum_{n=-\infty}^{\infty} g_n(z; x', z') \, \mathrm{e}^{-\frac{\mathrm{i}2\pi nx}{a}} \qquad \text{(A4)}$$

it follows that

$$\left(\frac{\partial^2}{\partial x^2} + \frac{\partial^2}{\partial z^2} \right) G(x, z; x', z') = \sum_{n=-\infty}^{\infty} \left(\frac{\mathrm{d}^2 g_n}{\mathrm{d}z^2} - \frac{n^2 4\pi^2}{a^2} g_n \right) \mathrm{e}^{-\frac{\mathrm{i}2\pi nx}{a}} \quad \text{(A5)}$$

Similarly, expanding the x-part of the Dirac-delta function into a Fourier series:

$$\delta(x - x') = \sum_{n=-\infty}^{\infty} \left\{ \frac{1}{a} \int_0^a \delta(x - x') \, \mathrm{e}^{\frac{\mathrm{i}2\pi nx}{a}} \, \mathrm{d}x \right\} \mathrm{e}^{-\frac{\mathrm{i}2\pi nx}{a}}$$

$$= \frac{1}{a} \sum_{n=-\infty}^{\infty} \mathrm{e}^{\frac{\mathrm{i}2\pi nx'}{a}} \mathrm{e}^{-\frac{\mathrm{i}2\pi nx}{a}} \qquad \text{(A6)}$$

it follows, from (A1), (A5), (A6) and the orthogonality of the Fourier terms, that

$$\frac{\mathrm{d}^2 g_n}{\mathrm{d}z^2} - \frac{n^2 4\pi^2}{a^2} g_n = -\frac{1}{a} \mathrm{e}^{\frac{\mathrm{i}2\pi nx'}{a}} \delta(z - z'), \quad n = -\infty \ldots \infty \qquad \text{(A7)}$$

Let g_n^+ and g_n^- be the solutions to (A7) in the regions $z > z'$ and $z < z'$, respectively. At $z = z'$, the Dirac-delta term yields a step-discontinuity

in $\frac{\mathrm{d}g_n}{\mathrm{d}z}$ while g_n becomes continuous. Hence, one obtains the boundary conditions

$$g_n^+\left(z';x',z'\right) = g_n^-\left(z';x',z'\right) \tag{A8}$$

$$\frac{\mathrm{d}g_n^+}{\mathrm{d}z}\left(z';x',z'\right) - \frac{\mathrm{d}g_n^-}{\mathrm{d}z}\left(z';x',z'\right) = -\frac{1}{a}\mathrm{e}^{\frac{\mathrm{i}2\pi nx'}{a}} \tag{A9}$$

For $n = 0$, one obtains

$$g_0^+ = A_0^+ + B_0^+ z = A_0^+ + \frac{B_0^+ + B_0^-}{2}z + \frac{B_0^+ - B_0^-}{2}z \tag{A10}$$

$$g_0^- = A_0^- + B_0^- z = A_0^- + \frac{B_0^+ + B_0^-}{2}z - \frac{B_0^+ - B_0^-}{2}z \tag{A11}$$

The common term $\frac{B_0^+ + B_0^-}{2}z$ gives rise to a homogeneous field with sources at $z = \pm\infty$, and since this kind of field is absent we have $B_0^- = -B_0^+$, whereby (A9) yields

$$B_0^+ = -\frac{1}{2a}, \qquad B_0^- = \frac{1}{2a} \tag{A12}$$

Using (A8), we thus obtain

$$A_0^- = A_0^+ - \frac{z'}{a}$$

Since any additive constant does not influence the field, we can impose the additional condition $g_0(z';x',z') = 0$, which yields $A_0^+ = -A_0^- = \frac{z'}{2a}$ whereby

$$g_0\left(z;x',z'\right) = -\frac{|z - z'|}{2a} \tag{A13}$$

For $n \neq 0$ we disregard solutions giving rise to fields that grow without bound when $|z| \to \infty$. Hence

$$g_n^+ = A_n^+\mathrm{e}^{-\frac{2\pi|n|z}{a}}, \qquad g_n^- = A_n^-\mathrm{e}^{\frac{2\pi|n|z}{a}}, \tag{A14}$$

for which (A8) and (A9) yield

$$A_n^+ = \frac{1}{4\pi|n|}\mathrm{e}^{\frac{\mathrm{i}2\pi nx'}{a}}\mathrm{e}^{\frac{2\pi|n|z'}{a}}, \qquad A_n^- = \frac{1}{4\pi|n|}\mathrm{e}^{\frac{\mathrm{i}2\pi nx'}{a}}\mathrm{e}^{-\frac{2\pi|n|z'}{a}} \tag{A15}$$

Collecting all terms, the Fourier expansion of the periodic Green's function becomes

$$G\left(x,z;x',z'\right) = -\frac{|z - z'|}{2a} + \frac{1}{4\pi}\sum_{n\neq 0}\frac{1}{|n|}\mathrm{e}^{-\frac{\mathrm{i}2\pi nx}{a}}\mathrm{e}^{\frac{\mathrm{i}2\pi nx'}{a}}\mathrm{e}^{-\frac{2\pi|n||z-z'|}{a}} \tag{A16}$$

Finally, since the Green's function is real valued, the expansion is rewritten to

$$G\big(x, z; x', z'\big) = -\frac{|z - z'|}{2a} + \frac{1}{2\pi} \sum_{n=0}^{\infty} \frac{1}{n} \left[\cos\left(\frac{2\pi n x}{a}\right) \cos\left(\frac{2\pi n x'}{a}\right) \right.$$

$$\left. + \sin\left(\frac{2\pi n x}{a}\right) \sin\left(\frac{2\pi n x'}{a}\right) \right] e^{-\frac{2\pi n |z - z'|}{a}} \qquad \text{(A17)}$$

In our particular problem, we have

$$\boldsymbol{M}_0(x) = M_{\mathrm{S}} \left[\cos\left(\frac{2\pi x}{a}\right) \hat{\boldsymbol{x}} + \sin\left(\frac{2\pi x}{a}\right) \hat{\boldsymbol{y}} \right], \quad 0 < z < d,$$

with $\boldsymbol{M}_0 = \boldsymbol{0}$ elsewhere, which yields

$$\rho_{\mathrm{m}}(x) = -\nabla \cdot \boldsymbol{M}_0 = \frac{2\pi}{a} M \sin\left(\frac{2\pi x}{a}\right), \quad 0 < z < d, \ \ \text{(A18)}$$

$\sigma_{\mathrm{m}}(z = 0) = -\hat{\boldsymbol{z}} \cdot \boldsymbol{M}_0 = 0$, $\sigma_{\mathrm{m}}(z = d) = \hat{\boldsymbol{z}} \cdot \boldsymbol{M}_0 = 0$, and $\rho_{\mathrm{m}} = \sigma_{\mathrm{m}} = 0$ elsewhere.

By using (A3), we thus obtain

$$\Psi_0(x, z) = \frac{M_{\mathrm{S}}}{2} \sin\left(\frac{2\pi x}{a}\right) \int_0^d e^{-\frac{2\pi |z - z'|}{a}} \mathrm{d}z'$$

$$= \frac{M_{\mathrm{S}} a}{2\pi} \sin\left(\frac{2\pi x}{a}\right) \begin{cases} \sinh\left(\frac{\pi d}{a}\right) e^{-\frac{2\pi}{a}\left(z - \frac{d}{2}\right)}, & z > d \\ 1 - e^{-\frac{\pi d}{a}} \cosh\left(\frac{2\pi}{a}\left(z - \frac{d}{2}\right)\right), & 0 < z < d \quad \text{(A19)} \\ \sinh\left(\frac{\pi d}{a}\right) e^{\frac{2\pi}{a}\left(z - \frac{d}{2}\right)}, & z < 0 \end{cases}$$

from which $\boldsymbol{H}_0 = -\nabla \Psi_0$ becomes

$$H_{0,x}(x, z) = M_{\mathrm{S}} \cos\left(\frac{2\pi x}{a}\right) \begin{cases} -\sinh\left(\frac{\pi d}{a}\right) e^{-\frac{2\pi}{a}\left(z - \frac{d}{2}\right)}, & z > d \\ e^{-\frac{\pi d}{a}} \cosh\left(\frac{2\pi}{a}\left(z - \frac{d}{2}\right)\right) - 1, & 0 < z < d \quad \text{(A20)} \\ -\sinh\left(\frac{\pi d}{a}\right) e^{\frac{2\pi}{a}\left(z - \frac{d}{2}\right)}, & z < 0 \end{cases}$$

$$H_{0,y}(x, z) = 0 \qquad \qquad \qquad \qquad \qquad \qquad \qquad \text{(A21)}$$

$$H_{0,z}(x, z) = M_{\mathrm{S}} \sin\left(\frac{2\pi x}{a}\right) \begin{cases} \sinh\left(\frac{\pi d}{a}\right) e^{-\frac{2\pi}{a}\left(z - \frac{d}{2}\right)}, & z > d \\ e^{-\frac{\pi d}{a}} \sinh\left(\frac{2\pi}{a}\left(z - \frac{d}{2}\right)\right), & 0 < z < d \quad \text{(A22)} \\ -\sinh\left(\frac{\pi d}{a}\right) e^{\frac{2\pi}{a}\left(z - \frac{d}{2}\right)}, & z < 0 \end{cases}$$

Assuming that $\frac{\pi d}{a} \ll 1$, *i.e.*, a thin layer, and including the first order terms, the field inside the magnetized layer becomes

$$\boldsymbol{H}_0 \approx M_{\mathrm{S}} \left[-\frac{\pi d}{a} \cos\left(\frac{2\pi x}{a}\right) \hat{\boldsymbol{x}} + \frac{2\pi}{a}\left(z - \frac{d}{2}\right) \sin\left(\frac{2\pi x}{a}\right) \hat{\boldsymbol{z}} \right] \quad \text{(A23)}$$

APPENDIX B. EXPRESSIONS FOR THE MATRICES USED IN THE SCATTERING ANALYSIS

The sub-matrices in the fundamental Equation (44) are given by

$$\mathbf{W}_{11} = \begin{pmatrix} -\mathrm{i}k_{0y}\mathbf{p}^6 - \mathrm{i}\mathbf{k} & \mathrm{i}\mathbf{p}^7\mathbf{k} - \mathrm{i}\mathbf{k} \\ \mathrm{i}k_{0y}\mathbf{p}^1 - \mathrm{i}k_{0y}\mathbf{I} & -\mathrm{i}\mathbf{p}^1\mathbf{k} - \mathrm{i}k_{0y}\mathbf{I} \end{pmatrix} \quad \text{(B1)}$$

$$\mathbf{W}_{12} = \begin{pmatrix} \mathrm{i}\omega\mu_0\mathbf{p}^8 + \mathrm{i}\dfrac{k_{0y}}{\omega\varepsilon_0\varepsilon}\mathbf{k} & \mathrm{i}\omega\mu_0\mathbf{p}^9 - \mathrm{i}\dfrac{1}{\omega\varepsilon_0\varepsilon}\mathbf{kk} \\ -\mathrm{i}\omega\mu_0\mathbf{p}^2 + \mathrm{i}\dfrac{k_{0y}}{\omega\varepsilon_0\varepsilon}\mathbf{I} & -\mathrm{i}\omega\mu_0\mathbf{p}^3 - \mathrm{i}\dfrac{k_{0y}}{\omega\varepsilon_0\varepsilon}\mathbf{k} \end{pmatrix} \quad \text{(B2)}$$

$$\mathbf{W}_{21} = \begin{pmatrix} -\mathrm{i}\dfrac{k_{0y}}{\omega\mu_0}\mathbf{k}\boldsymbol{\mu}_{33}^{-1} & -\mathrm{i}\omega\varepsilon_0\varepsilon\mathbf{I} + \mathrm{i}\dfrac{1}{\omega\mu_0}\mathbf{k}\boldsymbol{\mu}_{33}^{-1}\mathbf{k} \\ \mathrm{i}\omega\varepsilon_0\varepsilon\mathbf{I} - \mathrm{i}\dfrac{k_{0y}^2}{\omega\mu_0}\boldsymbol{\mu}_{33}^{-1} & +\mathrm{i}\dfrac{k_{0y}}{\omega\mu_0}\boldsymbol{\mu}_{33}^{-1}\mathbf{k} \end{pmatrix} \quad \text{(B3)}$$

$$\mathbf{W}_{22} = \begin{pmatrix} \mathrm{i}k_{0y}\mathbf{I} - \mathrm{i}\mathbf{k}\mathbf{p}^{10} & \mathrm{i}\mathbf{k} - \mathrm{i}\mathbf{k}\mathbf{p}^{11} \\ \mathrm{i}k_{0y}\mathbf{I} - \mathrm{i}k_{0y}\mathbf{p}^4 & -\mathrm{i}\mathbf{k} - \mathrm{i}k_{0y}\mathbf{p}^5 \end{pmatrix} \quad \text{(B4)}$$

where

$$\mathbf{p}^i = \begin{pmatrix} p_0^i & \cdots & p_{2N}^i \\ \vdots & \ddots & \vdots \\ p_{-2N}^i & \cdots & p_0^i \end{pmatrix}, \quad \mathbf{k} = \begin{pmatrix} k_{x,-N} & \cdots & 0 \\ \vdots & \ddots & \vdots \\ 0 & \cdots & k_{x,N} \end{pmatrix} \quad \text{(B5)}$$

with

$$p_n^1 = \frac{1}{a}\int_0^a \mu_{33}^{-1}\mu_{13}\mathrm{e}^{-\mathrm{i}n\frac{2\pi}{a}x}dx,$$

$$p_n^2 = \frac{1}{a}\int_0^a \left(\mu_{11} - \mu_{13}\mu_{33}^{-1}\mu_{31}\right)\mathrm{e}^{-\mathrm{i}n\frac{2\pi}{a}x}dx \quad \text{(B6)}$$

$$p_n^3 = \frac{1}{a}\int_0^a \left(\mu_{12} - \mu_{13}\mu_{33}^{-1}\mu_{32}\right)\mathrm{e}^{-\mathrm{i}n\frac{2\pi}{a}x}dx,$$

$$p_n^4 = \frac{1}{a}\int_0^a \mu_{33}^{-1}\mu_{31}\mathrm{e}^{-\mathrm{i}n\frac{2\pi}{a}x}dx \quad \text{(B7)}$$

$$p_n^5 = \frac{1}{a} \int_0^a \mu_{33}^{-1} \mu_{32} \mathrm{e}^{-\mathrm{i}n\frac{2\pi}{a}x} dx,$$

$$p_n^6 = \frac{1}{a} \int_0^a \mu_{33}^{-1} \mu_{23} \mathrm{e}^{-\mathrm{i}n\frac{2\pi}{a}x} dx = p_n^7 \tag{B8}$$

$$p_n^8 = \frac{1}{a} \int_0^a \left(\mu_{21} - \mu_{23}\mu_{33}^{-1}\mu_{31} \right) \mathrm{e}^{-\mathrm{i}n\frac{2\pi}{a}x} dx,$$

$$p_n^9 = \frac{1}{a} \int_0^a \left(\mu_{22} - \mu_{23}\mu_{33}^{-1}\mu_{32} \right) \mathrm{e}^{-\mathrm{i}n\frac{2\pi}{a}x} dx \tag{B9}$$

$$p_n^{10} = \frac{1}{a} \int_0^a \mu_{33}^{-1} \mu_{31} \mathrm{e}^{-\mathrm{i}n\frac{2\pi}{a}x} dx, \; p_n^{11} = \frac{1}{a} \int_0^a \mu_{33}^{-1} \mu_{32} \mathrm{e}^{-\mathrm{i}n\frac{2\pi}{a}x} dx \tag{B10}$$

$$k_{x,n} = k_{0x} + n\frac{2\pi}{a} \tag{B11}$$

The rotation matrix $\mathbf{\Phi}$ transforms between the main coordinate system and the plane of incidence, with respect to which the TM- and TE-type Floquet-modes in the free space region are defined:

$$\mathbf{\Phi} = \begin{pmatrix} \begin{pmatrix} \cos\varphi_{-N} & \cdots & 0 \\ \vdots & \ddots & \vdots \\ 0 & \cdots & \cos\varphi_N \end{pmatrix} & \begin{pmatrix} \sin\varphi_{-N} & \cdots & 0 \\ \vdots & \ddots & \vdots \\ 0 & \cdots & \sin\varphi_N \end{pmatrix} \\ \begin{pmatrix} -\sin\varphi_{-N} & \cdots & 0 \\ \vdots & \ddots & \vdots \\ 0 & \cdots & -\sin\varphi_N \end{pmatrix} & \begin{pmatrix} \cos\varphi_{-N} & \cdots & 0 \\ \vdots & \ddots & \vdots \\ 0 & \cdots & \cos\varphi_N \end{pmatrix} \end{pmatrix} \tag{B12}$$

where

$$\cos\varphi_n = \frac{k_{x,n}}{\left(k_{x,n}^2 + k_{y0}^2\right)^{1/2}}, \quad \sin\varphi_n = \frac{k_{y0}}{\left(k_{x,n}^2 + k_{y0}^2\right)^{1/2}} \tag{B13}$$

The impedance matrix $\mathbf{Z}$ gives the relation between the tangential fields of the Floquet-modes in the free space region:

$$\mathbf{Z} = \begin{pmatrix} \begin{pmatrix} 0 & \cdots & 0 \\ \vdots & \ddots & \vdots \\ 0 & \cdots & 0 \end{pmatrix} & \begin{pmatrix} Z_{\mathrm{TM},-N} & \cdots & 0 \\ \vdots & \ddots & \vdots \\ 0 & \cdots & Z_{\mathrm{TM},N} \end{pmatrix} \\ \begin{pmatrix} -Z_{\mathrm{TE},-N} & \cdots & 0 \\ \vdots & \ddots & \vdots \\ 0 & \cdots & -Z_{\mathrm{TE},N} \end{pmatrix} & \begin{pmatrix} 0 & \cdots & 0 \\ \vdots & \ddots & \vdots \\ 0 & \cdots & 0 \end{pmatrix} \end{pmatrix} \tag{B14}$$

where

$$Z_{\text{TM,n}} = \eta_0 \frac{k_{z,n}}{k_0}, \quad Z_{\text{TE,n}} = \eta_0 \frac{k_0}{k_{z,n}} \tag{B15}$$

$$k_{z,n} = \begin{cases} \left(k_0^2 - k_{x,n}^2 - k_{y0}^2\right)^{1/2}, & \text{when } k_{x,n}^2 + k_{y0}^2 \leq k_0^2 \\ \mathrm{i} \left(k_{x,n}^2 + k_{y0}^2 - k_0^2\right)^{1/2}, & \text{when } k_{x,n}^2 + k_{y0}^2 > k_0^2 \end{cases} \tag{B16}$$

REFERENCES

1. Knott, E. F., J. F. Shaeffer, and M. T. Tuley, *Radar Cross Section*, SciTech Publishing Inc., 5601 N. Hawthorne Way, Raleigh, NC 27613, 2004.

2. Iakubov, I., A. Lagarkov, S. Maklakov, A. Osipov, K. Rozanov, I. Ryzhikov, and S. Starostenko, "Microwave permeability of laminates with thin Fe-based films," *J. Magn. Magn. Mater.*, Vol. 272, 2004.

3. Rozanov, K., I. Iakubov, A. Lagarkov, S. Maklakov, A. Osipov, D. Petrov, I. Ryzhikov, M. V. Sedova, and S. Starostenko, "Laminates of thin ferromagnetic films for microwave applications," *The Sixth International Kharkov Symposium*, Vol. 1, 168–173, 2007.

4. Gilbert, T. L., "A phenomenological theory of damping in ferromagnetic materials," *IEEE Trans. Magnetics*, Vol. 40, 3443–3449, Nov. 2004.

5. Acher, O., P. L. Gourrierec, G. Perrin, P. Baclet, and O. Roblin, "Demonstration of anisotropic composites with tuneable microwave permeability manufactured from ferromagnetic thin films," *IEEE Trans. Microwave Theory Tech.*, Vol. 44, 674–684, 1996.

6. Ramprecht, J. and D. Sjöberg, "Biased magnetic materials in RAM applications," *Progress In Electromagnetics Research*, PIER 75, 85–117, 2007.

7. Huo, S., J. Bishop, J. Tucker, W. Rainforth, and H. Davies, "Simulation of 3-D micromagnetic structures in thin iron platelet," *IEEE Trans. Magnetics*, Vol. 33, 4170–4172, 1997.

8. Bagneres, A., "Three-dimensional numerical simulations of stripe chopping in a magnetic perpendicular material," *IEEE Trans. Magnetics*, Vol. 35, 4318–4325, 1999.

9. Redjdal, M., A. Kakay, M. Ruane, and F. Humphrey, "Cross-tie walls in thin permalloy films," *IEEE Trans. Magnetics*, Vol. 38, 2471–2473, 2002.

10. Steyskal, H., J. Ramprecht, and H. Holter, "Spiral elements for

broad-band phased arrays," *IEEE Trans. Antennas Propagat.*, Vol. 53, No. 8, 2558–2562, 2005.

11. Landau, L. D. and E. M. Lifshitz, "On the theory of the dispersion of magnetic permeability in ferromagnetic bodies," *Physik. Z. Sowjetunion*, Vol. 8, 153–169, 1935.

12. Landau, L. D. and E. M. Lifshitz, "On the theory of the dispersion of magnetic permeability in ferromagnetic bodies," *Collected Papers of L. D. Landau*, D. Ter Haar (ed.), 101–114, Reprinted by Gordon and Breach, Science Publishers, 1965.

13. Kittel, C., *Introduction to Solid State Physics*, 7th edition, John Wiley & Sons, New York, 1996.

14. Brown, W. F., *Micromagnetics*, Interscience Publishers, New York, 1963.

15. d'Aquino, M., "Nonlinear magnetization dynamics in thin-films and nanoparticles," Ph.D. thesis, Universita degli studi di Napoli "Federico II", Facolta di Ingegneria, Dec. 2004.

16. Pozar, D. M., *Microwave Engineering*, John Wiley & Sons, 3rd edition, New York, 2005.

17. Forslund, O. and S. He, "Electromagnetic scattering from an inhomogeneous grating using a wave-splitting approach," *Progress In Electromagnetics Research*, PIER 19, 147–171, 1998.

18. Rikte, S., G. Kristensson, and M. Andersson, "Propagation in bianisotropic media-reflection and transmission," *IEE Proc. Microwaves, Antennas and Propagation*, Vol. 148, No. 1, 29–36, 2001.

19. Kristensson, G., "Homogenization of corrugated interfaces in electromagnetics," *Progress In Electromagnetics Research*, PIER 55, 1–31, 2005.